Advanced Doubly Fed Induction Machine Rotor Fault Diagnosis Based on Wavelet Analysis in Closed-Loop Operation Under Time–varying Condition

Y. Gritli[1,2], A. Stefani[2], C. Rossi[2], F. Filippetti[2] and A. Chatti[1]

[1] National Institute of Applied Sciences and Technology
I.N.S.A.T., 7th November University at Carthage, Tunis (Tunisia)
Phone number: +216 71 703 717 – p.6057/6056
e-mail: **yasser.gritli@esti.rnu.tn, abderrazak.chatti@insat.rnu.tn**

[2] University of Bologna, Department of Electrical Engineering Bologna (Italy)
Phone/Fax number: +39 051 20 93 564 / +39 051 209 3588
e-mail: **andrea.stefani@mail.ing.unibo.it**, **claudio.rossi@ mail.ing.unibo.it,**
fiorenzo.filippetti@mail.ing.unibo.it

Abstract. This paper introduces a new diagnostic technique for the detection of incipient electrical rotor faults in doubly fed induction Machine (DFIM) for wind power systems. In the considered application, the rotor is supplied by a static converter for the control of active and reactive power flows from the generator to the electrical grid. A new diagnostic method based on the rotor modulating signals pre-processing by Frequency Sliding (FS) and Discrete Wavelet Transform (DWT) thereby is here proposed to detect rotor faults dynamically over time. Experimental and simulation results demonstrate the effectiveness of the proposed approach under time-varying conditions.

Key words

Doubly Fed Induction Machine (DFIM), rotor fault, Sliding Frequency (SF), Wavelet decomposition.

1. Introduction

Wind power generation has become the most accessible and efficient form of renewable energy during the past few years. Wind turbines equipped with Doubly Fed Induction Machine (DFIM) are emerging as the preferred technology in the field. Among different alternatives and for Variable Speed Constant Frequency (VSCF) generation systems, the DFIM can provide higher energy output with lower rating of power converter. Particularly in this type of application, monitoring the induction machine is crucial to ensure safe operation, timely maintenance and increased operation reliability for extracting the maximum of the wind energy. A recent study [1] has revealed that 13% of wind turbine failures are related to the motor. Investigations on different failure modes in induction motors have revealed that 19% of the overall motor faults are related to the rotor part [2]. A detailed analysis of this type of fault can be found in [3]. Different diagnostic methods have been proposed for wind turbines using DFIM [4]–[6]. Depending on wind speed, the induction machine operates continuously in time-varying condition. In this context, the classical application of Fourier Analysis (FA) for processing manipulated (voltages) or controlled (currents) variables fails as slip and speed vary. Thus the fault components are spread in a bandwidth proportional to the variation. Among different solutions, high resolution frequency estimation [7] and more recently Signal Demodulation (SD) technique [8] have been developed to reduce the effect of the non periodicity on the analyzed signals. These techniques, based on (FA) give high quality discrimination between healthy and faulty conditions but don't provide time domain information. Wavelets, on the other hand, provide greater resolution in time for high frequency components of a signal and greater resolution in frequency for low frequency components. This method has been used with different approaches for the diagnosis of anomalies in induction machine [9]–[12]. Most of the reported contributions are based on the wavelet analysis of currents during start-up or load variation for diagnosis purposes. In this context, the frequency components are spread in a wide bandwidth as slip and speed vary considerably. This fact justifies the common use of multi-detail or/and approximation signals resulting from wavelet decomposition, whose levels are imposed by the sampling frequency. This dependency on the appropriate choice of the sampling frequency and tracking multi fault frequency components on multi frequency bands complicate the diagnosis process. Moreover, the use of large frequency bands subjects the detection procedure to erroneous interpretations due to possible confusion with other harmonics due to the use of gearboxes [13], commonly used in wind turbines. Motivated by the above discussion, a new monitoring and diagnostic technique based on frequency sliding and DWT thereby, has been investigated in open-loop operation and experimentally validated [14]-[15]. Obviously in open-loop case, rotor voltages have no values due to the short circuited rotor windings. In closed-loop drives, the control itself has an

impact on the relevance of fault frequency components on both manipulated (voltages) and controlled (currents) variables [16]. In this paper, rotor currents and voltages will be analysed to evaluate this impact in time-varying condition and to prove the robustness of the proposed technique in discriminating healthy from faulty rotor in DFIM.

2. Control System Description

For a DFIM associated with a back-to-back PWM converter on the rotor side and with the stator directly connected to the grid, a stator flux oriented vector control is utilized in order to control separately the active and reactive power on the stator side. The relationships between the active and reactive stator power and the rotor current components are [5]:

$$P_s \cong -\frac{3}{2} \cdot |\overline{v_s}| \cdot \frac{L_m}{L_s} i_{qr} \qquad (1)$$

$$Q_s \cong \frac{3}{2} \cdot |\overline{v_s}| \cdot \frac{L_m}{L_s} \left(\frac{|\overline{v_s}|}{2\pi f_s L_m} - i_{dr} \right) \qquad (2)$$

Where L_s and L_m are the stator inductance and the magnetizing inductance respectively. Equations (1) and (2) show the possibility to realize a decoupled power control. In fact the stator active power is in inverse proportion with the quadrature rotor current i_{qr}, and that the stator reactive power is in inverse proportion with the direct rotor current i_{dr}, being the stator voltage and frequency $/v_s/$ and f_s imposed by the grid.
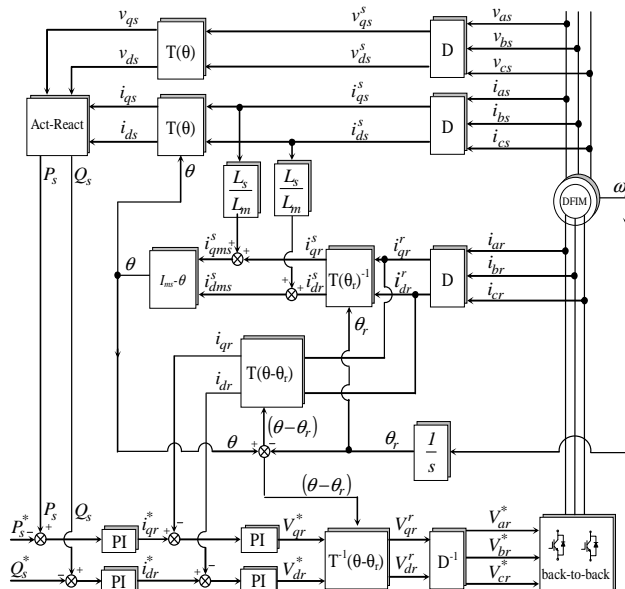

Fig. 1. Block scheme of the whole control system

As shown in Fig. 1. the DFIM control system is based on two cascaded loops. The outer loop is dedicated to the stator active and reactive power control, whereas the inner one is related to the direct and quadrature rotor current components. The blocks containing D and D^{-1} represents respectively the Clarke's and the inverse Clarke's transformations from a three phase to a two phase dq system. On the other hand those containing $T(\theta)$, $T(\theta-\theta_r)$, $T^{-1}(\theta)$, $T^{-1}(\theta-\theta_r)$ represents the reference

frame transformations respectively from stationary (stator) to synchronous, from rotating (rotor) to synchronous and their inverse, being θ and θ_r the stator flux phase angle and the rotor position angle respectively. The control algorithm uses the components of the magnetizing current space vector [5] to compute the phase θ of the stator flux vector by means of the following equation:

$$\theta = \arctan\left(\frac{i_{qms}}{i_{dms}} \right) \qquad (3)$$

Moreover in order to increase the accuracy in the angle computation a complex digital filter was applied to the magnetizing current components in the stator reference frame i_{qms} and i_{dms} appearing in the equation (3). On the other hand the rotor position angle θ_r is retrieved thanks to an incremental encoder present in the control system.

3. Rotor fault frequency tracking – The proposed approach

The principal feature of wavelet analysis is its High Multiresolution Analysis HMRA capability. Wavelet analysis is signal decomposition, using successive combination of approximation and detail signals. The procedure is repeated until the original signal is decomposed to a pre-defined J level decomposition [17].
With the well known dyadic down sampling procedure, frequency bands of each level of decomposition are related to the sampling frequency. Hence, these bands can't be changed unless a new acquisition with different sampling frequency is made. This fact complicates any fault detection based on DWT, particularly in time-varying condition. In this paper, an efficient solution to overcome this limitation is proposed. With a sampling frequency $fs=3.2kHz$, an eight level decomposition ($J=8$) was chosen in order to cover the frequency bands in which we can track frequency component characteristics of the fault (see Table I).
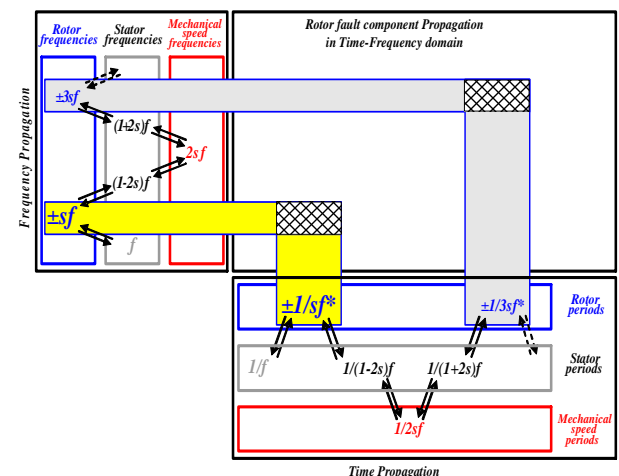

Fig. 2 Time-Frequency propagation of a rotor fault: the sign (–) in time domain is corresponding to the inverse current sequence component.

Under healthy conditions, only the fundamental frequencies sf exist on rotor currents and voltages (f:

supply frequency, *s:* slip). Observing the time-frequency propagation of a rotor fault illustrated in Fig. 2, the first fault frequency component that occurs in the rotor currents and voltages is *–sf*. Neglecting other effects like slotting and saturation, it can be assumed that the major components of the rotor current and voltage space vectors can be written respectively as:

$$\underline{i_r}(t) = \sqrt{3}\left[Ie^{j\omega_r t} + I_{-sf}\,e^{j(\omega_{-sf}t - \varphi_{-sf})} + I_{3sf}\,e^{j(\omega_{3sf}t - \varphi_{3sf})}\right] (4)$$

$$\underline{V_r}(t) = \sqrt{3}\left[Ve^{j\omega_r t} + V_{-sf}\,e^{j(\omega_{-sf}t - \varphi_{-sf})} + V_{3sf}\,e^{j(\omega_{3sf}t - \varphi_{3sf})}\right] (5)$$

Where *I* and *V* are the rms values of the fundamental component, (I, V_{-sf} and I, V_{3sf}) are those relatively to the first and second level of fault harmonic components $\omega_{-sf} = -s\omega$ and $\omega_{3f} = 3s\omega$. In time varying conditions the magnitudes I_{sf}, V_{-sf}, I_{3sf} and V_{3sf} can't be detected through a frequency analysis since ω_{-sf} and ω_{3sf} are spread in a wide frequency range.

A simple processing of the rotor current space vector, allows shifting the fault component *-sf* to a desired prefixed frequency band. In such a way, all the information related to the fault is isolated and confined in a single frequency band. More in detail, a frequency sliding with f_{sl} is applied at each time slice to the rotor current and voltages space vectors as in (6), so that the harmonic component of interest is moved to the desired frequency band. Then the real part of the shifted signal is analyzed by means of DWT.

$$I, V_{sl}(t) = \mathrm{Re}\left[\underline{i_r}, \underline{V_r}(t)e^{-j2\pi f_{sl}t}\right] (6)$$

The choice of f_{sl} is done for shifting the fault frequency component in one of the intervals $[0 : 2^{-(J+1)}\cdot f_s]$ or $[2^{-(J+1)}\cdot f_s : 2^{-J}\cdot f_s]$ and subsequently the DWT is applied to analyze the frequency band of interest. The proposed approach was applied to the rotor current and voltages space vectors with f_{sl}=-8.5Hz, to isolate the contribution of the *-sf* component. Hence, with respect to the frequency bands reported in Table I, the frequency band of interest, for tracking the *-sf* frequency contribution is the 8th DWT level decomposition.

Table I. – Frequency Band of each level

Approximations «a_i»	Frequency Bands (Hz)	Details «d_i»	Frequency bands (Hz)
a_8	: [0 – 6.25]	d_8	: [6.25 – 12.5]
a_7	: [0 – 12.5]	d_7	: [12.5 – 25]
a_6	: [0 – 25]	d_6	: [25 – 50]
a_5	: [0 – 50]	d_5	: [50 – 100]
a_4	: [0 – 100]	d_4	: [100 – 200]

4. Rotor fault analysis under speed-varying condition

A. Simulation results

In order to validate the applicability of the proposed diagnostic approach, several simulations, under healthy and faulty rotor conditions, were conducted. Rotor unbalance was emulated by inserting an additional resistance *Radd* in series with one rotor phase winding.
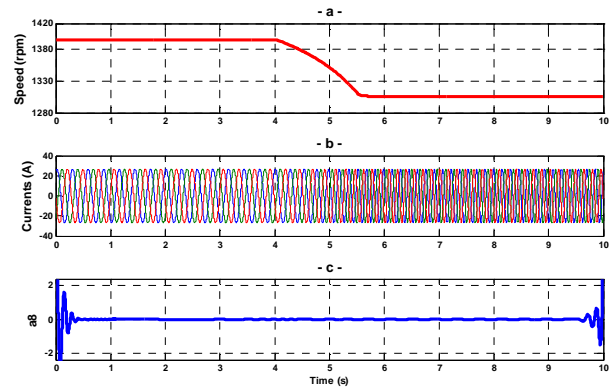

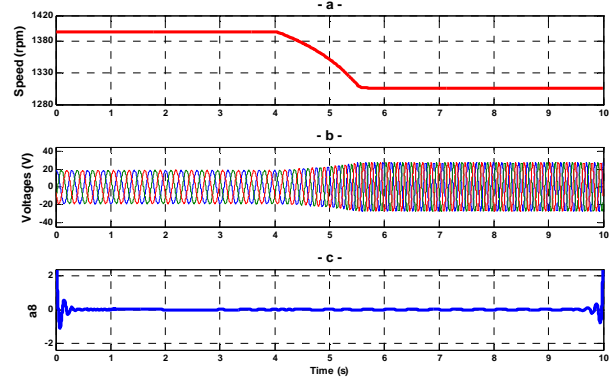Fig. 3. DWT of the rotor current I_{sl} in healthy condition (Radd=0) under speed transient. Simulation results

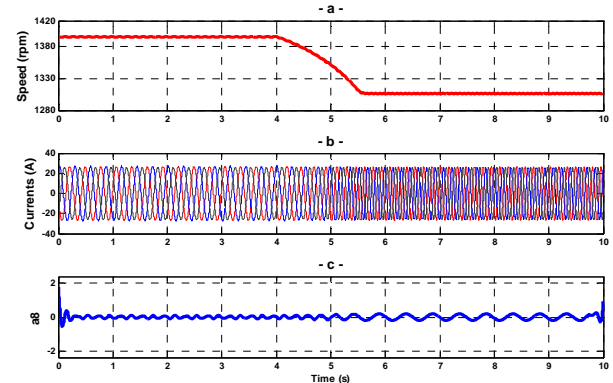Fig. 4. DWT of the rotor voltage V_{sl} in healthy condition (Radd=0) under speed transient. Simulation results

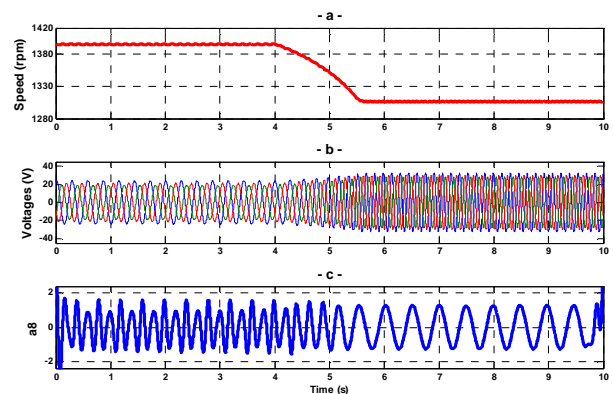Fig. 5. DWT of the rotor current I_{sl} in faulty condition (Radd=Rr) under speed transient. Simulation results

Fig. 6. DWT of the rotor voltage V_{sl} in faulty condition (Radd=Rr) under speed transient. Simulation results

The controlled machine has been initially simulated in healthy condition (Radd=0), with a bandwidth of the current loop equal to *Bp=100 Hz* and with the generator delivering an active power of 5500W and absorbing a reactive power of 4100 VAR from the stator side, during a prefixed transient from 1395 rpm to 1306 rpm. All signals reported have been recorded during 10 seconds.

As explained in the previous section, the contribution of the fault frequency components –*sf* will be observed on approximation a_8 after a suitable frequency sliding applied to the rotor current and then the voltage space vectors.

The wavelet decompositions of the I_{sl} and V_{sl} signals, in healthy condition during deceleration, are used as a reference in comparison with the faulty case. In Fig. 3-c and Fig. 4-c, the 8th approximation signal (relatively to I_{sl} and V_{sl}) for healthy machine is depicted. It is possible to notice that no effect on these signals, during the speed transient, has been registered. In faulty condition (Radd=Rs), the contribution of the –*sf* component, observed on the 8th approximation signal, is more relevant for the rotor voltages (Fig.6-c) than the corresponding one to the rotor current (Fig.5-c).The loss of relevance observed on rotor currents is mainly due to the damping effect of the control system imposed by the bandwidth of the current loop.

B.   Experimental results

In order to validate the results obtained in simulations, a test bed was realized. A 5.5 kW 2 poles pair wound rotor induction machine (see Appendix) was connected with a PWM back to back converter on the rotor side (see Appendix). The direct field oriented control for the DFIM was implemented on a dSPACE DS1103 board. The generator was coupled with a 9 kW DC motor fed by a commercial DC/DC chopper converter controlled in speed used to test and reproduce the simulated speed transients.
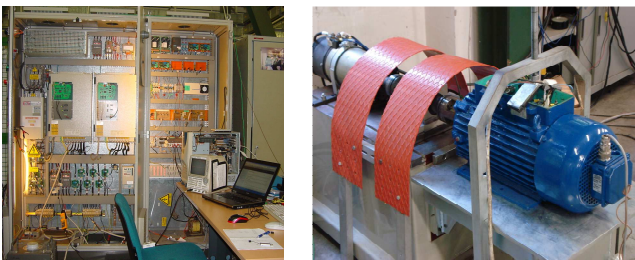

Fig. 7 Experimental test bed photos

Experimental test bed photos are illustrated in Fig. 7. For the study of the phenomena caused by a rotor fault, an external resistance *Radd* has been inserted in series to one rotor phase in order to emulate rotor asymmetry. Experimental results under healthy and faulty conditions *(Radd=Rr)* are reported from Fig. 8 to Fig. 11. These results corroborate simulations although the magnitude evolutions in some cases are even bigger than in simulation.

The 8th approximation signal obtained from the experimental results show the sensitivity and the effectiveness of this particular approximation signal to reproduce the contribution of the frequency component -*sf* under rotor unbalance.
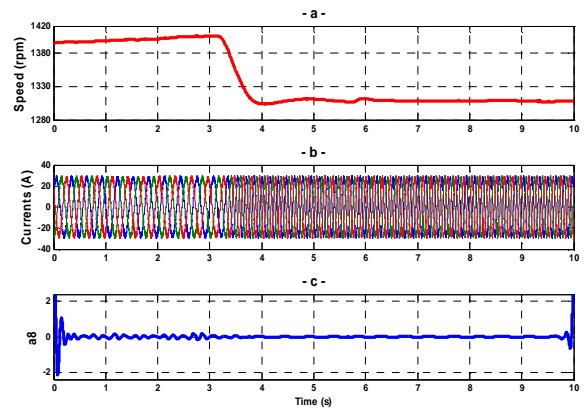

Fig. 8. DWT of the rotor current I_{sl} in healthy condition (Radd=0) under speed transient. Experimental results

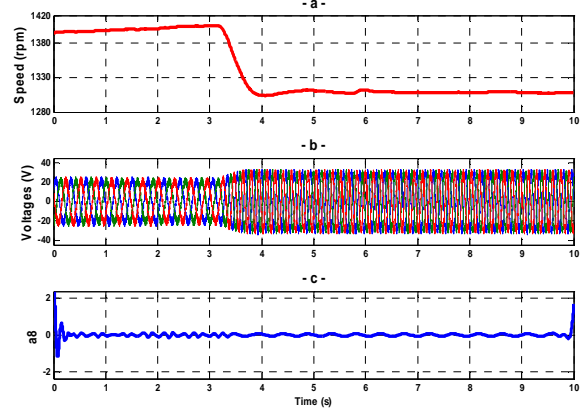
Fig. 9. DWT of the rotor voltage V_{sl} in healthy condition (Radd=0) under speed transient. Experimental results
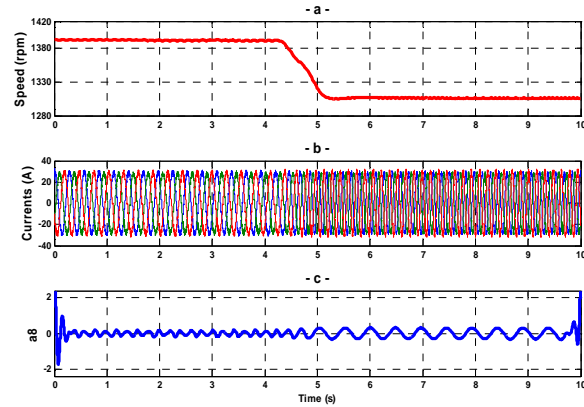

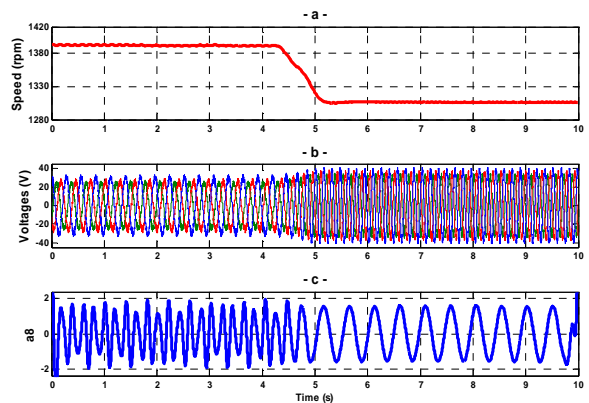Fig. 10. DWT of the rotor current I_{sl} in faulty condition (Radd=Rr) under speed transient. Experimental results

Fig. 11. DWT of the rotor voltage V_{sl} in faulty condition (Radd=Rr) under speed transient. Experimental results

5. Quantitative rotor fault evaluation

Once the state of the machine has been qualitatively diagnosed, a quantitative evaluation of the fault degree is necessary. For these purposes a dynamic multiresolution mean power indicator mPa_j at different resolution levels j was introduced as a diagnostic index to quantify the extent of the fault as in (7):

$$mPa_j(I,V) = \frac{1}{N} \sum_{n=1}^{N} \left| a_j(n) \right|^2 \tag{7}$$

Where N is the number of samples and j is the level decomposition. In this way, for J level wavelet decomposition, we construct a J dimensional feature vector for future analysis. Since the most relevant fault frequency component is the $-sf$ only its contribution clamped in the 8th approximation a_8 was adopted to quantify the extent of the fault.

Other fault components could be treated in the same way but they are neglected because of the damping effect of the machine load and inertia on higher order fault harmonics. This choice reduces the feature dimension and consequently the computational time.

The fault indicator is periodically calculated (every 400 samples) using a window of 1600 samples as depicted in Fig. 12 where δn=400 samples and Δn=1600 samples.
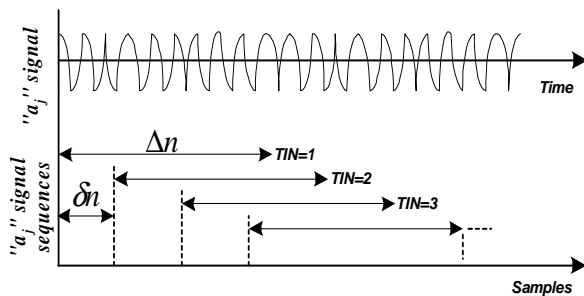

Fig. 12. Principle of time interval calculation,
TIN: Time Interval Number

These values were regulated experimentally to reduce variations that can lead to false alarm in healthy operating conditions of the motor. When the fault occurs, the energy distribution of the signal is changed at the resolution levels related to the characteristic frequency bands of the default. Hence, the energy excess confined in the approximation is considered as an anomaly indication in case of rotor faults.

The mean power of the approximation a_8 resulting from the wavelet decomposition applied to rotor currents and voltages, which have been obtained from simulations (Fig. 3 and Fig. 5) are depicted in Fig.13-a and Fig.13-b respectively. In healthy conditions ($Radd=0$) and under large range of speed variations, the calculated $mPa_8(I,V)$ indicators don't show any significant changes. Consequently, the indicator values for the healthy motor response are considered as a baseline to set the threshold for discriminating healthy from unbalanced rotor conditions. In faulty conditions ($Radd=Rr$) the calculated $mPa_8(I)$ indicator (Fig. 13-a) don't show significant increase. As previously discussed, this is due to the damping effect of the control system. However, the calculated $mPa_8(V)$ indicator (Fig. 13-a) show significant

increase. The large energy deviation observed in faulty conditions prove the effectiveness of the proposed approach, since the speed motor operation does not disturb the assessment with respect to the case of a healthy machine. Experimental results under healthy and faulty conditions ($Radd=Rr$) are depicted in Fig. 14. The slight oscillation observed on the fault indicator in Fig. 13-b and Fig. 14-b comes from the proximity of the fault frequency $-sf$ to the fundamental one sf of the rotor voltages. This fact together with the intrinsic overlapping effects of wavelet transformation causes this oscillation. Anyway the results that have been obtained experimentally corroborate simulations although the magnitude evolutions in some cases are even bigger than in simulation, thus proving the effectiveness of the proposed time-frequency rotor fault indicator.
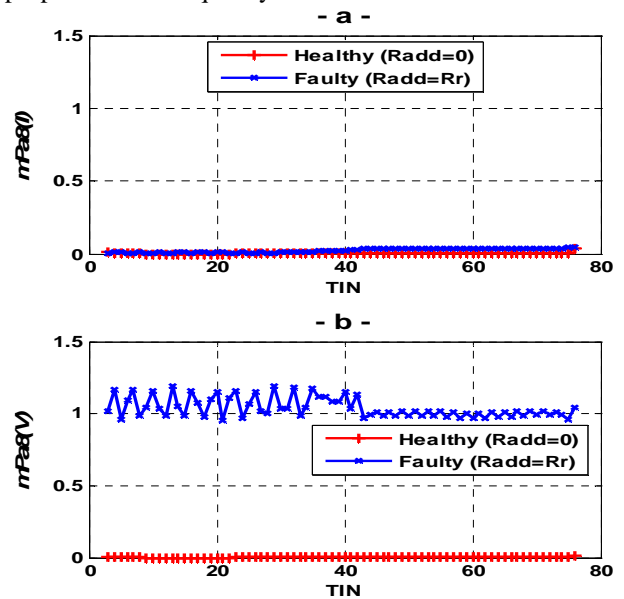

Fig. 13. Mean power of the approximation a8 resulting from the wavelet decomposition of the signals I_{sl} (-a-) and V_{sl} (-b-) under deceleration transient. Simulation results.
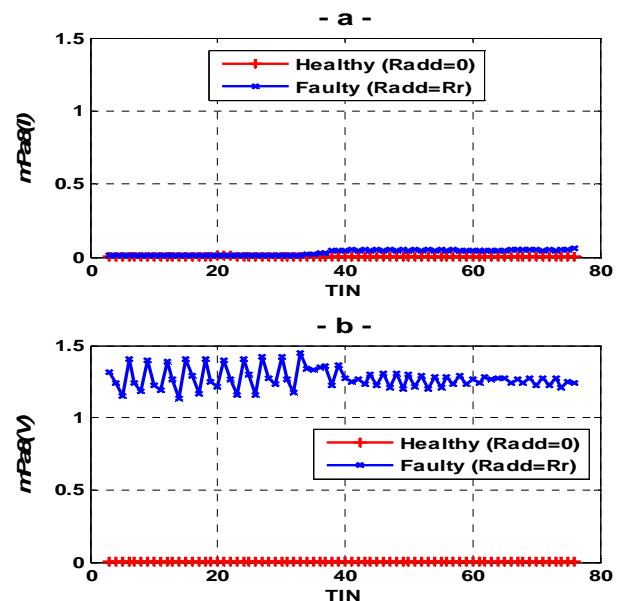

Fig. 14. Mean power of the approximation a_8 resulting from the wavelet decomposition of the signals I_{sl} (-a-) and V_{sl} (-b-) under deceleration transient. Experimental results.

6. Conclusion

The aim of this paper was to validate the effectiveness of a new and reliable approach for the characterization of rotor fault in time varying condition.The proposed approach is based on an optimized use of the DWT by a simple pre-processing of the variables to be analyzed. Results prove that for closed loop condition and under a rotor unbalance, rotor voltages are more sensitive than rotor currents. These results show the limits of the current signature analysis under time-varying conditions. A dynamic time-frequency fault indicator is presented to quantify the fault extent. Simulation and experimental results carried out, demonstrate the effectiveness of this new approach that can be applied to any type of machine and extended for diagnosing other types of faults under time–varying conditions.

APPENDIX

Induction Motor Parameters

Parameter		Value
Rated Power	kW	5.5
Rated stator/	V	380
rotor voltage	V	186
Rated frequency	Hz	50
Rated speed	rpm	1400
Stator phase resistance	Ω	0.531
Rotor phase resistance	Ω	0.310
Stator inductance	H	0.083
Rotor inductance	H	0.019
Mutual inductance	H	0.038
Pole pairs		2

Back-to-Back Converter

Parameter		Value
Gride side converter switching frequency	kHz	10
Rotor side converter switching frequency	kHz	12
Gride voltage	V	400
Gride coupling inductance	mH	1.2
DC-Link voltage	V	500
Encoder type	Imp/tun	1024

References

[1] F. Ciamberlano, J. Nitschke, N. Kragelund, J. Thiede, M. Fusselbaugh, M. Johst, F.V. Velde, "Engineering Insurance of Offshore Wind Turbines", 39th IMIA Annual Conference on Sept. 2006 in Boston.

[2] A.H. Bonnett, C. Yung,, "Increased Efficiency Versus Increased Reliability", IEEE Ind. App. Mag., Vol. 14, Issue 1, Jan./Feb. 2008

[3] A. Bellini, F. Filippetti, C. Tassoni, and G. A. Capolino, "Advances in diagnostic Techniques for induction machines", IEEE Tran. on Ind. Elec., Vol.55, N° 12, Dec. 2008.

[4] V. Dinkhauser, F.W. Fuchs, "Rotor turn-to-turn faults of doubly-fed Induction generators in wind energy plants-modelling, simulation and detection", 13th EPE-PEMC'08, pp. 1819–1826, Sept. 2008.

[5] A. Stefani, A. Yazidi, C. Rossi, F. Filippetti, D. Casadei and G.A. Capolino, "Doubly Fed Induction Machines Diagnosis Based on Signature Analysis of Rotor Modulating Signals", IEEE Trans. on Indus. Appl., Vol. 44, N° 6, Nov/Dec 2008.

[6] Y. Gritli, A. Stefani, F. Filippetti and A. Chatti, "Stator fault analysis based on Wavelet technique for wind turbines equipped with DFIG", ICCEP'09, pp 485-491. Italy, June 2009.

[7] Kia, S.H.; Henao, H.; Capolino, G.-A., "A High-Resolution Frequency Estimation Method for Three-Phase Induction Machine Fault Detection", IEEE Tran. Ind. Elec, Vol. 54, Issue 4, pp. 2305 – 2314, Aug. 2007.

[8] A. Stefani, F. Filippetti, A. Bellini, "Diagnosis of Induction Machines in Time-varying Conditions", IEEE Trans. on Ind. Appl., Vol. 56, N° 11, Nov. 2009.

[9] S. Rajagopalan, J.M. Aller, J.A. Restrepo, T.G. Habetler, R.G. Harley, "Analytic-Wavelet-Ridge-Based Detection of Dynamic Eccentricity in Brushless Direct Current (BLDC) Motors Functioning Under Dynamic Operating Conditions", IEEE Trans. on Ind. Elec, Vol. 54, N° 3, pp. 1410–1419, June 2007.

[10] A. Ordaz-Moreno, R.J.Romero-Troncoso, J. A. Vite-Frias, J. R. Rivera-Gillen, and A. Garcia-Perez, "Automatic Online Diagnosis Algorithm for Broken-Bar Detection on Induction Motors Based on Discrete Wavelet Transform for FPGA Implementation", IEEE Trans. on Ind. Elec., Vol. 55, N° 5, pp. 1361–1368, May. 2008.

[11] J. Cusido, L. Romeral, J.A. Ortega, J.A. Rosero, A. G. Espinosa, "Fault Detection in Induction Machines Using Power Spectral Density in Wavelet Decomposition", IEEE Trans. Ind. Elec., Vol. 55, N° 2, pp. 633–643, Feb. 2008.

[12] J.A. Daviu, P.J. Rodriguez, M.R. Guasp, M. P. Sanchez, A. Arkkio, "Detection of combined faults in induction machines with stator parallel branches through the DWT of the start-up current", Journal of Mechanical Systems and Signal Processing, accepted in Feb. 2009.

[13] W.T. Thomson and M. Fenger, "Current Signature Analysis to Detect Induction Motor Faults", IEEE Industry Applications Magazine, pp. 26-34, July/August 2001.

[14] Y. Gritli, A. Stefani, C. Rossi, F. Filippetti and A. Chatti, "Doubly Fed Induction Machine Stator fault Diagnosis Under Time-Varying Conditions Based on Frequency Sliding and Wavelet Analysis", IEEE-SDEMPED'09. Cargese-France, Aug./Sep. 2009.

[15] Y. Gritli, A. Stefani, A. Chatti, C. Rossi and F. Filippetti, " The Combined use of the Instantaneous Fault Frequency Evolution and Frequency Sliding for Advanced Rotor Fault Diagnosis in DFIM Under Time-Varying Condition", IECON'09. Porto-Portugal, Nov. 2009.

[16] D. Casadei, F. Filippetti, C. Rossi and A. Stefani, "Closed Loop Bandwidth Impact on Doubly Fed Induction Machine Asymmetries Detection Based on Rotor Voltage Signature Analysis", 43rd UPEC'08, Padova-Italy, Sept. 2008.

[17] T.K. Sarkar, C. Su, R. Adve, M.S. Palma, L.G. Castillo, R. Boix, "A Tutorial on Wavelets from an Electrical Engineering Perspective, Part 1: Discrete Wavelet Techniques", IEEE Ante. and Prop. Mag., Vol. 40, N° 5, Oct. 1998.